Complete ^1H and ^{13}C Assignments of Coenzyme B_{12} through the Use of New Two-Dimensional NMR Experiments

Michael F. Summers,† Luigi G. Marzilli,‡ and Ad Bax*§

Contribution from the Biophysics Laboratory, Division of Biochemistry and Biophysics, Food and Drug Administration, Bethesda, Maryland 20892, the Department of Chemistry, Emory University, Atlanta, Georgia 30322, and the Laboratory of Chemical Physics, National Institute of Arthritis, Diabetes and Digestive and Kidney Diseases, National Institutes of Health, Bethesda, Maryland 20892. *Received February 3, 1986*

Abstract: Four different types of new two-dimensional (2D) NMR techniques have been used to determine unambiguous ^1H and ^{13}C spectral assignments for (5′-deoxyadenosyl)cobalamin (coenzyme B_{12}, M_r 1580, 6.5-mg sample in 0.35 mL of ^2H_2O). Two-dimensional homonuclear Hartmann–Hahn spectroscopy in combination with 2D spin-locked NOE spectroscopy was used to assign the resonances of all nonexchangeable protons. Sensitivity enhanced ^1H-detected 2D multiple-quantum NMR then provided the resonance assignments for all protonated ^{13}C nuclei. The resonance assignments for nonprotonated carbons were determined via ^1H–^{13}C multiple-bond, multiple-quantum spectroscopy. This experiment also confirmed independently our ^1H and ^{13}C assignments made with the other methods. The relative intensity of long-range ^1H–^{13}C correlations is related to the magnitude of the J_{CH} coupling involved and therefore provides qualitative structural information. Despite the careful application of classical ^{13}C NMR assignment techniques in recent reports on coenzyme B_{12}, we found that nearly one-third of the ^{13}C resonances had been assigned erroneously.

Since the early 1970s, cobalamins have been the subject of extensive NMR studies.[1-8] ^1H and ^{13}C resonance assignments have been used in the interpretation of steric and electronic effects and for structural analyses.[1,2] These resonance assignments were based on comparison with B_{12} analogues and related model compounds, interpretation of ^{13}C relaxation times, analyses of line-broadening effects in the presence of paramagnetic relaxation agents, pH effects, and heteronuclear scalar couplings. Assignments based on such evidence are susceptible to error; and as we will demonstrate in this paper, this approach can lead to erroneous conclusions for molecules as complex as cobalamins. In fact, despite the careful nature of earlier studies, nearly one-third of the ^{13}C NMR resonances of (5′-deoxyadenosyl)cobalamin (coenzyme B_{12}, Chart I) are reassigned, as reported here.

Two-dimensional NMR methods can greatly simplify the analysis of complex ^1H and ^{13}C spectra. However, the low solubility of coenzyme B_{12} makes the use of regular heteronuclear ^1H–^{13}C experiments difficult. It is shown here that this problem can be overcome easily by using ^1H-detected heteronuclear multiple-quantum coherence via direct coupling (HMQC)[9-14] or via multiple-bond coupling.[15] This approach alleviates the ^{13}C sensitivity problem by at least an order of magnitude. Another problem in the NMR study of coenzyme B_{12} is that nuclear Overhauser effects (NOEs) are very weak at the magnetic field strength employed. This is due to the size of the molecule, which has a molecular tumbling time, τ_c, close to $1/\omega_L$, where ω_L is the angular proton Larmor frequency. Thus, the 2D NOESY experiment[16,17] that normally provides valuable "through-space connectivity" often gives poor results for molecules with molecular weights in the range of 1000–2000. In this study, we use the spin-locked NOE experiment, recently proposed by Bothner-By et al.,[18] to obtain the NOE information in a more effective way. This experiment provides the crucial connection between the J-coupled fragments of the molecule that are not connected via homonuclear ^1H coupling. Proton resonance assignments within each fragment could then, in principle, be established by using the well-known homonuclear correlated spectroscopy (COSY) method.[19-21] However, because of the severe spectral overlap in several regions of the ^1H spectrum, we find the recently developed homonuclear Hartmann–Hahn (HOHAHA) method[22-25] preferable. This sensitive technique provides high-resolution phase-sensitive spectra that display both direct and relayed connectivities.

Chart I

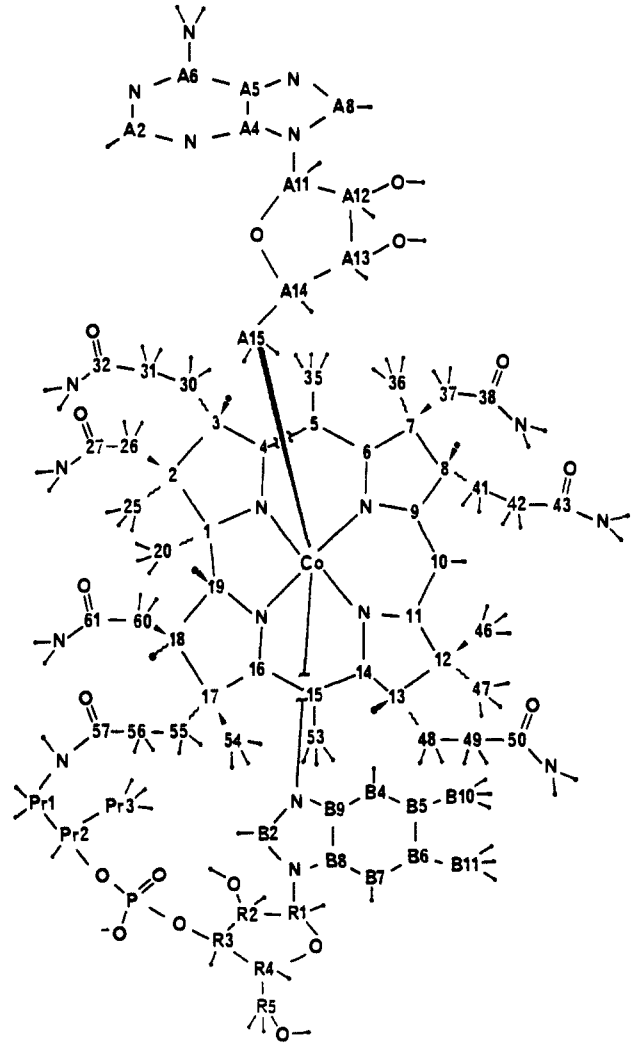

Combined use of the techniques mentioned above provides a new and reliable procedure for assignment of complex ^1H and ^{13}C

* Author to whom correspondence should be addressed.
† Food and Drug Administration.
‡ Emory University.
§ National Institutes of Health.

(1) Bratt, G. T.; Hogenkamp, H. P. C. *Biochemistry* **1984**, *23*, 5653 and references therein.

0002-7863/86/1508-4285$01.50/0 © 1986 American Chemical Society

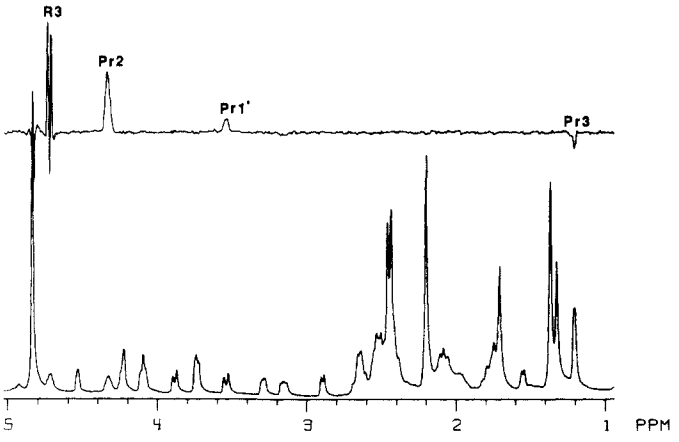

Figure 1. Part of the regular ^1H spectrum of coenzyme B_{12} (bottom) and ^1H–^{31}P spin–echo difference spectrum (top). In the top spectrum, only protons that have a scalar interaction with the ^{31}P nucleus are present.

NMR spectra. This approach involves (a) assignment of the ^1H spectrum using HOHAHA, COSY, spin-locked NOE, and ^1H–^{31}P spin–echo difference methods; (b) correlation via $^1J_{CH}$ to provide the ^{13}C assignments for protonated carbons; and (c) correlation via $^2J_{CH}$ and $^3J_{CH}$ to provide assignments of nonprotonated carbons and to independently verify ^1H and ^{13}C assignments made with the other methods. All experiments were carried out using a relatively small amount of sample (6.5 mg), requiring special attention to be paid to the optimization of the experimental parameters for the various types of newer 2D NMR techniques.

Assignment of the ^1H NMR Spectrum

A ^1H–^{31}P echo difference spectrum[27,28], using the sequence

^1H $\quad 90°_x$–Δ–$180°_x$–Δ–Acq.(±)

^{31}P $\quad 90°_x 90°_{\pm x}$ decouple

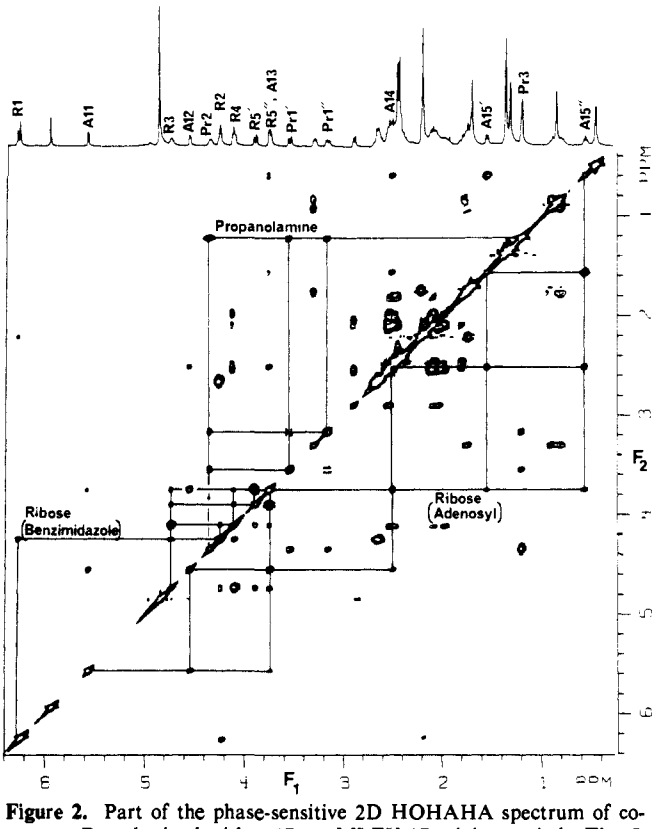

Figure 2. Part of the phase-sensitive 2D HOHAHA spectrum of coenzyme B_{12}, obtained with a 57-ms MLEV-17 mixing period. The *J*-connectivity patterns for the two ribose rings and the propanolamine protons are indicated in the figure by drawn lines. Other connectivity patterns are indicated in supplementary figures.

is used to identify protons that are coupled to the ^{31}P nucleus. Figure 1 shows the difference spectrum obtained for coenzyme B_{12} and identifies protons R3H and Pr2H plus low intensity resonances that will later be identified as Pr3H′ and Pr3H. Hydrogens are identified by the carbon atom to which they are attached; for magnetically nonequivalent geminal protons, H′ and H″ refer to the protons with the downfield and upfield chemical shift, respectively. The R3H and Pr2H protons provide a simple starting point for further assignments which then can be made on the basis of NOE and scalar connectivity.

Homonuclear Hartmann–Hahn Spectroscopy. The recently developed HOHAHA method[22–26] is used for defining the scalar-coupled networks. The sequence used here is

$$90_\phi\text{–}t_1\text{–}SL_x(\text{MLEV-17})_N SL_x\text{–Acq.}(t_2)$$

where SL_x denotes a short (2.5 ms) spin lock field applied along the x axis (to defocus magnetization transverse to the x axis), and the phase ϕ is cycled along all four axes as described elsewhere.[29,30] The MLEV-17 sequence[25] is repeated an integer number of times, N. We prefer use of the MLEV-17 version over other types of propagation schemes for the following reasons. (a) A substantial bandwidth (>4 kHz) can be covered by using a modest rf field strength (7 kHz). (b) The apparent $T_{1\rho}$ can be prolonged by up to a factor of 2.[25,26] This makes the method attractive for larger molecules that generally have short T_2 and $T_{1\rho}$ values. (c) The MLEV mixing sequence attenuates magnetization transfer that can occur via spin-locked NOE.[18,31] This magnetization transfer is attenuated because during the MLEV sequence the "spin-locked" magnetization is aligned approximately 50% of the time along the static magnetic field. For molecules that are not in the

(2) Hensen, O. D.; Hill, H. A. O.; McClelland, C. E.; Williams, R. J. P. In *B12*; Dolphin, D., Ed.; Wiley: New York, 1982; Vol. 1, p 463 and references therein.
(3) Hogenkamp, H. P. C.; Tkachuck, R. D.; Grand, M. E.; Fuentes, R.; Matwiyoff, N. A. *Biochemistry* **1975**, *14*, 3707.
(4) Dixon, R. M.; Golding, B. T.; Howarth, O. W.; Murphy, J. L. *J. Chem. Soc., Chem. Commun.* **1983**, 243.
(5) Alcock, N. W.; Dixon, R. M.; Golding, B. T. *J. Chem. Soc., Chem. Commun.* **1985**, 603.
(6) Ernst, L. *J. Chem. Soc., Perkin Trans 1* 1984, 2267.
(7) Benn, R.; Mynott, R. *Angew. Chem., Int. Ed. Engl.* **1985**, *24*, 333.
(8) Rossi, M.; Glusker, J. P.; Randaccio, L.; Summers, M. F.; Toscano, P. J.; Marzilli, L. G. *J. Am. Chem. Soc.* **1985**, *107*, 1729. Brown, K. L.; Hakimi, J. M.; Jacobson, D. W. *J. Am. Chem. Soc.* **1984**, *106*, 7894. Brown, K. L.; Hakimi, J. M. *J. Am. Chem. Soc.* **1986**, *108*, 496.
(9) Muller, L. *J. Am. Chem. Soc.* **1979**, *101*, 4481.
(10) Bax, A.; Griffey, R. G.; Hawkins, B. L. *J. Am. Chem. Soc.* **1983**, *105*, 7188.
(11) Bax, A.; Griffey, R. G.; Hawkins, B. L. *J. Magn. Reson.* **1983**, *55*, 301.
(12) Live, D. H.; Davis, D. G.; Agosta, W. C.; Cowburn, D. *J. Am. Chem. Soc.* **1984**, *106*, 6104.
(13) Bendall, M. R.; Pegg, D. T.; Doddrell, D. M. *J. Magn. Reson.* **1983**, *52*, 81.
(14) Bax, A.; Subramanian, S. *J. Magn. Reson.* **1986**, *67*, 565.
(15) Bax, A.; Summers, M. F. *J. Am. Chem. Soc.* **1986**, *108*, 2093.
(16) Jeener, J.; Meier, B. H.; Bachmann, P.; Ernst, R. R. *J. Chem. Phys.* **1979**, *71*, 4546.
(17) Macura, S.; Ernst, R. R. *Mol. Phys.* **1980**, *41*, 1980.
(18) Bothner-By, A. A.; Stephens, R. L.; Lee, J. T.; Warren, C. D.; Jeanloz, R. W. *J. Am. Chem. Soc.* **1984**, *106*, 811.
(19) Aue, W. P.; Bartholdi, E.; Ernst, R. R. *J. Chem. Phys.* **1976**, *64*, 2229.
(20) Bax, A.; Freeman, R. *J. Magn. Reson.* **1981**, *42*, 542.
(21) Rance, M.; Sorensen, O. W.; Bodenhausen, G.; Wagner, G.; Ernst, R. R.; Wuthrick, K. *Biochem. Biophys. Res.Commun.* **1983**, *117*, 479.
(22) Braunschweiler, L.; Ernst, R. P. *J. Magn. Reson.* **1983**, *53*, 521.
(23) Davis, D. G.; Bax, A. *J. Am. Chem. Soc.* **1985**, *107*, 2820.
(24) Davis, D. G.; Bax, A. *J. Am. Chem. Soc.* **1985**, *107*, 7197.
(25) Bax, A.; Davis, D. G. *J. Magn. Reson.* **1985**, *65*, 355.
(26) Bax, A.; Davis, D. G. In *Advanced Magnetic Resonance Techniques in Systems of High Molecular Complexity*; Nicolai, N., Valensin, G., Eds.; Birkhauser: Basel, in press.
(27) Freeman, R.; Mareci, T. H.; Morris, G. A. *J. Magn. Reson.* **1981**, *42*, 341.
(28) Cohen, J. S.; Chen, C.-W.; Bax, A. *J. Magn. Reson.* **1984**, *59*, 181.
(29) States, D. J.; Haberkorn, R. A.; Ruben, D. J. *J. Magn. Reson.* **1982**, *48*, 286.
(30) Bax, A. *Bull. Magn. Reson.* **1985**, *7*, 167.
(31) Bax, A.; Davis, D. G. *J. Magn. Reson.* **1985**, *63*, 207.

Table I. Summary of Observed NMR Connectivities in (5′-Deoxyadenosyl)cobalamin with the Homonuclear Hartmann–Hahn (HOHAHA), Spin-Locked NOE, and Heteronuclear Multiple-Bond Correlation (HMBC) Methods[a]

^1H signal	HOHAHA (^1H)	NOE (^1H)	HMBC	^1H signal	HOHAHA (^1H)	NOE (^1H)	HMBC
C20		B4; C18; C25; C30″; B2; C60[b]	C1: C2; C19	C55″	C55′; C56	C55′; C56	C57
				C56	C55	C55; C18; C54; C60	
C25		C3; C20; C30″; C26; C18; C60[b]	C1; C2; C3; C26	C18	C19;[b] C60[b]	C20; C55′; C56; C54; C19; C25	C1; C17; C19; C54; C60; C61[b]
C26		C3; C19; C25	C2; C27	C60	C19;[b] C18[b]	C19; C54; C20; C25; C55′; C56	C17; C18; C61;[b] C19
C3	C30; C31	C25; C26; C30′; C31; C35[c]	C1; C2; C26; C30; C31; C4	C19	C18;[b] C60[b]	A15′; C26; C54; C60; A14;[d] C18	
C30′	C30″; C31; C3	C3; B4; C30″	C32				
C30″	C30′; C31; C3	B4; C20; C25; C30′; C35	C32	Pr1′	Pr1″; Pr2; Pr3	Pr1″; Pr2; Pr3	Pr2; C57
C31′	C31″; C30; C3	C3	C30; C32	Pr1″	Pr1′; Pr2; Pr3	Pr1′; Pr2; Pr3	Pr2; C57
C31″	C31′; C30; C3	C3	C30; C32	Pr2	Pr1; Pr3	Pr1; Pr3	
C35		C36; B4; B10; C3; C30″; C37′	C4; C5; C6	Pr3	Pr1; Pr2	Pr1; Pr2	Pr1; Pr2
				R1	R2; R3; R4	B2; B7; R2; R3; R4	R2; B2
C36		B4; C35; C8; C37′	C6; C7; C8; C37	R2	R1; R3; R4	R1; R3; R4; C20; C48; B7	R1; R4
C37′	C37″	C37″, C36; C35	C7; C8; C38				
C37″	C37′	C37′; C8	C7; C38	R3	R2; R4; R5	R2; R5	R2; R5
C8	C41; C42	C41′; C36; C37″; C10	C6; C7; C9; C37; C41; C42	R4	R2; R3; R5	B2; R5	
				R5′	R5″; R3; R4	R5″; R3; R4	R3
C41′	C41″; C42; C8	C8; C41″; C42	C43	R5″	R5′; R3; R4	R5′; R3; R4	R3
C41″	C41′; C42; C8	C41′	C43	B4	B10	B10; C20; C30; C35; C36; C41″	B2; B6; B8; B10
C42	C41; C8	C41′	C43				
C10		C8; C41′; C42; C46; C47	C8; C9; C11; C12	B10	B4	B4; C35	B4; B6; B5
C46		C10; A11; C13; A14; C47	C11; C12; C13; C47	B11	B7	B7	B5; B7; B6
C47		C10; C46 C48″; C49; C13	C11; C12; C13; C46	B7	B11	R1; R2; B11	B5; B9; B11
C13	C48; C49	C46; C48′; C49; C53; C47	C11; C12; C14; C46; C48; C49	B2		R1; R4; C48; C20	B8; B9
				A2			A6
C48′	C48″; C49; C13	B2; C13; C49	C50	A8		A11; A12; A13	A4; A5
C48″	C48′; C49; C13	B2; C47; C49	C50	A11	A12; A13; A14	A8; A13; A14; C46; C54	A4; A8; A12
C49	C48; C13	C13; C47; C48	C13; C48; C50				
C53		C13; C54	C14; C15; C16	A12	A11; A13; A14	A8; A13; A14	A14
C54		A11; C19; C60; C53; C18; C55′; C56	C16; C17; C18; C55	A13	A11; A12; A14; A15	A8; A11; A12; A14; A15	A11; A12; A15
C55′	C55″; C56	C18; C55″; C56; C54; C60	C18	A14	A11; A12; A13; A15	A11; A12; A13; A15′; C46; C19	A13
				A15′	A15″; A13; A14	A13; A14; A15″; C19	
				A15″	A13; A14; A15	A13; A15′	

[a] Primes and double primes denote downfield and upfield ^1H signals, respectively, of geminal methylene protons; if absent, cross peaks include both proton signals. [b] C18 and C60 proton signals overlap. [c] C26 and C35 proton signals overlap. [d] A14 and C26 proton signals overlap.

extreme narrowing limit, the regular NOE is much smaller (or of opposite sign) than the spin-locked NOE, and therefore the average NOE observed during the MLEV sequence is strongly attenuated. (d) The rate at which magnetization is transferred between coupled spins during the MLEV mixing is identical with the rate for the other optimized versions of the HOHAHA experiment.[23,24] Suggestions on how to verify correct functioning of the sequence are given in the Practical Suggestions section.

During the mixing period of the HOHAHA experiment, magnetization propagates from one proton (A) to another (M) at a rate determined by the homonuclear scalar coupling (J_{AM}). If proton M is coupled to a third proton, X, the magnetization of A can be relayed via M to the X nucleus. For long mixing periods, magnetization from one proton will be redistributed over all other protons in the same coupling network, and intensities (and sensitivity) will be much lower than for relatively short mixing times. We use here an intermediate duration of 57 ms, sufficient to provide relay information but without severely decreasing the sensitivity of the experiment. The upfield region of the spectrum obtained this way, recorded in 1.5 h, is shown in Figure 2. The proton with a signal at 4.33 ppm, coupled to ^{31}P (Figure 1), shows connectivity to a methyl group at 1.21 ppm and two protons at 3.16 and 3.54 ppm. Two of these signals are observed also in the ^1H–^{31}P difference spectrum of Figure 1. Therefore, all these resonances correspond to the propanolamine moiety. Similarly, the other proton coupled to ^{31}P shows connectivities to all other protons of the ribose ring of the benzimidazole nucleotide. The adenosyl ribose protons also can be identified easily from Figure 2.

The connectivity networks for the corrin ring side chains are indicated in supplementary figures. All observed HOHAHA connectivities are presented in Table I. To assign the networks to a particular side chain, the spin-locked NOE experiment is used.

One disadvantage of the HOHAHA method is that it is sometimes difficult to determine whether a cross peak represents direct or relayed connectivity. To make this distinction one may also have to record a COSY spectrum or another HOHAHA spectrum with a shorter mixing time. For a mixing time of intermediate duration, as used for the spectrum of Figure 2, the assignments are largely unambiguous, however. Consider, for example, the adenosyl ribose ring. The anomeric proton, A11H, shows connectivity to A12H and A13H, but only A13H shows relayed connectivity to the A15 protons, distinguishing A12H and A13H unequivocally. As is the case with most homonuclear shift correlation methods (COSY, NOESY, and variations thereof), the intensities of two cross peaks at coordinates (δ_A,δ_B) and (δ_B,δ_A) can be different if (a) the acquisition times in the two time domains are different; (b) different digital filtering procedures are used in the two dimensions; or (c) if the longitudinal relaxation times, T_1, of spins A and B are different and the delay time between scans is not much longer (in practice a factor of 2) than the longest relaxation time of the two spins concerned. To minimize measuring time, a delay time of 1.5 times the *average* T_1 value of the protons is commonly used in homonuclear correlation methods. A delay time much shorter than this introduces artifacts and reduces sensitivity. Because the ribose protons R3H and R4H relax faster than anomeric proton R1H, weak relay peaks from R3H and R4H to R1H are observed, whereas the relay peaks from R1H and R3H and R4H fall just below the contour level (Figure 2). In addition, attenuation of spectral intensities close to the edges of the 2D spectrum in the F_2 dimension can be caused by the audiofrequency filters.

Spin-Locked NOE Spectroscopy. The spin-locked NOE experiment is employed for providing through-space connectivity

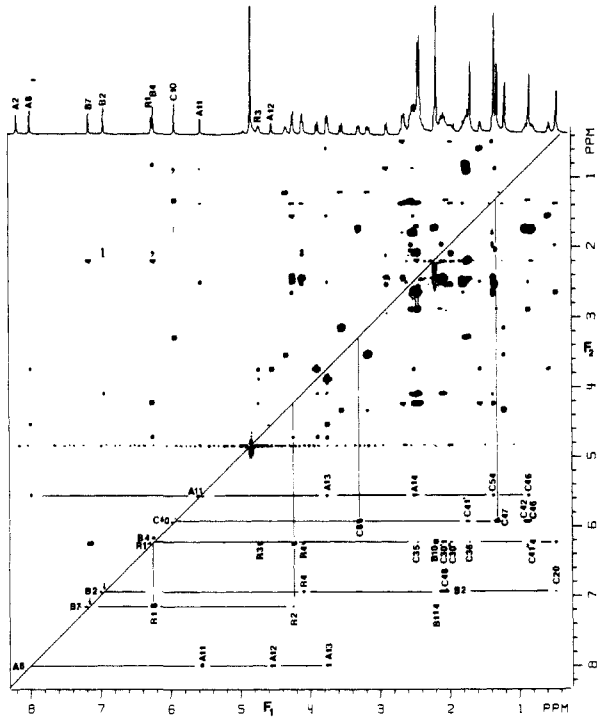

Figure 3. Part of the absorption mode 2D spin-locked NOE spectrum of coenzyme B_{12}, obtained with a 200-ms spin-lock period. Diagonal peaks are opposite in phase relative to cross peaks and are therefore not visible in this spectrum. Connectivity patterns for the low-field protons are indicated in the figure.

between the various networks of coupled protons. At a 11.75-T magnetic field strength, the regular 2D NOE experiment[16,17] resulted in very weak cross peaks due to the fact that the molecular tumbling time, τ_c, for coenzyme B_{12} is close to the reciprocal of the angular Larmor frequency, ω_L. At lower temperature (4 °C) substantial negative NOEs were observed but the solubility of coenzyme B_{12} was reduced dramatically. With the spin-locked NOE experiment, NOEs are always positive and become stronger with slower tumbling of the molecule.[18] A second major advantage of the spin-locked NOE experiment is that cross peaks due to relayed NOE (from spin A, via M to X) are in-phase with the diagonal peaks and are therefore readily distinguished from direct NOEs, which are inverted relative to the diagonal. A complete analysis of this effect will be presented elsewhere. It is important in the spin-locked NOE experiment to avoid artifacts that can be induced by the homonuclear Hartmann–Hahn effect.[31] These effects can be minimized by using a relatively weak rf field and positioning the carrier frequency in the downfield region of the spectrum. For more details, see the Practical Suggestions section.

Figure 3 shows the spin-locked NOE spectrum, obtained with a mixing time of 200 ms. Nearly one hundred NOE connectivities can be identified in this spectrum and are presented in Table I. Below, we will briefly outline the use of the NOE connectivities to complete the assignment of the ^1H spectrum. In the HOHAHA spectrum, two benzimidazole protons at 7.16 ppm (outside the spectral region shown in Figure 2) and 6.24 ppm show scalar connectivity to two overlapping methyl groups at 2.19 ppm. The downfield signal shows NOE cross peaks with the R1 and R2 protons and is assigned to B7H The other benzimidazole proton, which does not exhibit cross relaxation with the ribose ring but has cross peaks with corrin side-chain protons, is assigned to B4H. The signal at 6.95 ppm shows NOE connectivity with the R1 and R4 protons and is assigned to B2H. The A8 proton (8.00 ppm) is identified by the cross peaks with sugar protons A11H, A12H, and A13H. The most downfield proton signal (8.19 ppm) shows no NOE cross peaks and is therefore assigned to A2H. The remaining downfield singlet (5.93 ppm) is then assigned to C10H since this is the only remaining proton at a conjugated site in the molecule and also because it is the only remaining single proton which lacks J coupling to other protons.

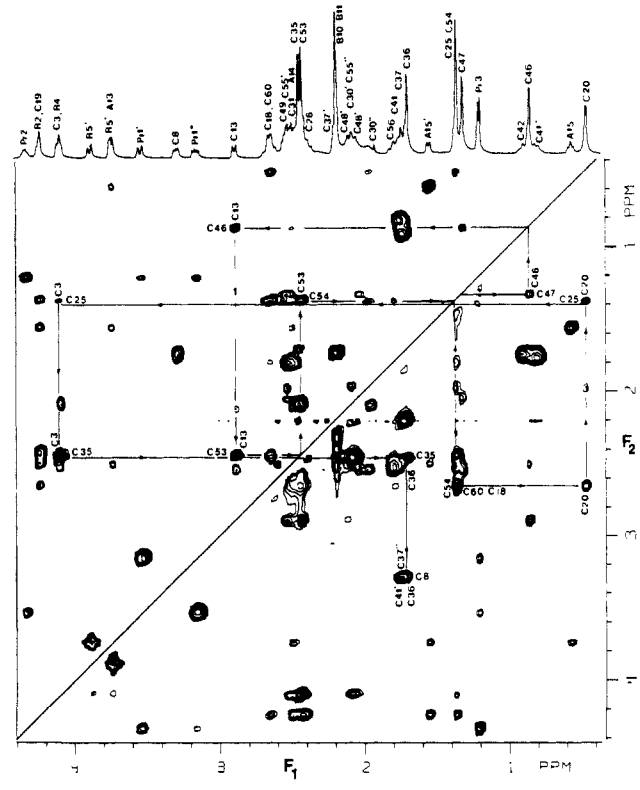

Figure 4. Expanded high-field region of the spectrum of Figure 3. The drawn lines indicate the NOE connectivity around the corrin ring, starting at methyl group C47, via protons C46, C13, C53, C54, C18, C20, C25, C3, C35, C36, to C8. Both the C8 and the C46 protons show NOE connectivity with C10 (Figure 3). Some asymmetry about the intense negative diagonal in the 1.5–2.5 ppm region is probably due to a small base-line distortion induced by overload of the receiver for the FID's recorded for the first few t_1 values.

The assignment of C10H provides a starting point for assignment of the remaining ^1H resonances. Without going into much detail, we will show how the spin-locked NOE spectrum can be used to connect the proton coupling networks of the corrin ring and its side chains. Figure 3 shows intense NOE connectivities between C10H and a proton at 3.29 ppm (C8H) and a methyl group at 1.32 ppm, which has to be either C46 or C47. As follows from the X-ray crystal structure data,[32] C47 is more proximate to C10H than C46, assigning the 1.32 ppm resonance to C47. As will be shown later, this assignment can also be made on the basis of long-range ^1H–^{13}C connectivity. Connectivities in the upfield region of the coenzyme are most easily observed in the expanded region of the spectrum, shown in Figure 4. Methyl protons C47 show connectivity to methyl protons C46, which have a cross peak with C13H. C13H shows connectivity to methyl protons C53, which show NOE connectivity to the C54 protons. Unfortunately, the resonances of methyl protons C54 and of another methyl group

(32) Lenhert, P. G.; Hodgkin, D. C. *Nature (London)* **1962**, *192*, 937.
(33) Maudsley, A. A.; Muller, L.; Ernst, R. R. *J. Magn. Reson.* **1977**, *28*, 463; Minoretti, A.; Aue, W. P.; Reinhold, M.; Ernst, R. R. *J. Magn. Reson.* **1980**, *40*, 175.
(34) Bodenhausen, G.; Ruben, D. J. *Chem. Phys. Lett.* **1980**, *69*, 185.
(35) Garbow, J. R.; Weitekamp, D. P.; Pines, A. *Chem. Phys. Lett.* **1982**, *93*, 504.
(36) Bax, A. *J. Magn. Reson.* **1983**, *52*, 330.
(37) Shaka, A. J.; Keeler, J.; Freeman, R. *J. Magn. Reson.* **1983**, *53*, 313.
(38) Kessler, H.; Griesinger, C.; Zarbock, J.; Loosli, H. R. *J. Magn. Reson.* **1984**, *57*, 331. Kessler, H.; Bermel, W.; Griesinger, c. *J. Am. Chem. Soc.* **1985**, *107*, 1083.
(39) Kogler, H.; Sorensen, O. W.; Bodenhausen, G.; Ernst, R. R. *J. Magn. Reson.* **1983**, *55*, 157.
(40) Frey, M. H.; Wagner, G.; Vasak, M.; Sorensen, O. W.; Neuhaus, D.; Worgotter, E.; Kagi, J. H. R.; Ernst, R. R.; Wuthrich, K. *J. Am. Chem. Soc.* **1985**, *107*, 6847.
(41) Nagayama, K.; Kumar, A.; Withrich, K.; Ernst, R. R. *J. Magn. Reson.* **1980**, *40*, 321.
(42) Bax, A.; Freeman, R.; Morris, G. A. *J. Magn. Reson.* **1981**, *42*, 164.

Table II. ^1H and ^{13}C NMR Chemical Shifts and Signal Assignments for (5'-Deoxyadenosyl)cobalamin[a]

assignment[b]	δ[c] ^{13}C NMR	δ[c] ^1H NMR	assignment[b]	δ[c] ^{13}C NMR	δ[c] ^1H NMR
C35 (C53)	18.3	2.45[d]	R3 (R3)	76.2	4.72[d]
C53 (C36)	18.8	2.43[d]	A13 (A12)	76.6	3.74
C54 (C54)	19.6	1.36[d]	C19 (C19)	76.8	4.24[d]
C25 (C35)	19.9	1.36[d]	R4 (R4)	84.6[f]	4.10[d]
C36 (C25)	21.7	1.70[d]	C1 (C1)	88.5	
Pr3 (Pr3)	21.7	1.21[d]	A14 (A14)	88.6	2.54
B11 (C46)	22.3	2.19[d]	R1 (R1)	89.4	6.26[d]
B10 (C20)	22.5	2.19[d]	A11 (A11)	91.0	5.56
C20 (B11)	23.5	0.47[d]	C10 (C10)	97.7	5.93[d]
C47 (B10)	23.9	1.32[d]	C15 (C15)	106.9	
A15 (A15)	27.3	1.55,[d] 0.57[d]	C5 (C5)	108.4	
C41 (C41)	28.7	1.75, 0.81	B7 (B7)	113.5	7.16[d]
C30 (C30)	29.2	2.06, 1.96	B4 (B4)	121.4	6.24[d]
C48 (C48)	30.3	2.22, 2.00	A5 (A5)	121.8	
C46 (C55)	34.2	0.87[d]	B8 (B8)	133.3	
C55 (C47)	34.4	2.45, 2.06	B5 (B6)	134.5	
C56 (C42)	34.6	1.78	B6 (B5)	136.8	
C60 (C60)	34.8	2.65	B9 (B9)	141.0	
C42 (C56)	34.8	0.88, 1.73	A8 (A8)	143.8	8.00
C49 (C49)	38.1	2.54	B2 (B2)	144.7	6.95[d]
C31 (C31)	38.3	2.50	A4 (A4)	151.8	
C18 (C18)	42.5	2.65	A2 (A2)	156.0	8.19
C37 (C26)	45.3	2.19, 1.72	A6 (A6)	158.7	
C26 (C37)	46.2	2.41	C6 (C6)	166.6	
Pr1 (Pr1)	47.8	3.54,[d] 3.16[d]	C14 (C14)	167.2	
C12 (C12)	49.5		C9 (C9)	173.1	
C2 (C2)	49.5		C11 (C11)	177.6	
C7 (C7)	53.1		C38 (C57)	177.9	
C13 (C13)	55.8	2.89	C57 (C38)	178.2	
C8 (C8)	57.5	3.29	C16 (C16)	178.7	
C3 (C3)	58.5	4.10	C4 (C4)	178.7	
C17 (C17)	60.8		C61 (C61)	179.0	
R5 (R5)	63.4	3.88,[d] 3.74[d]	C27 (C27)	179.3	
R2 (Pr2)	72.0	4.23[d]	C43 (C43)	180.3	
A12 (A13)	75.6	4.54	C32 (C32)	181.1	
Pr2 (R2)	76.0[e]	4.33[d]	C50 (C50)	181.1	

[a] The difference between ^{13}C shifts observed here (referenced to TSP) and reported earlier (referenced to neat Me_4Si) is 2.9 ppm. [b] Previous assignments (ref 1) are given in parentheses. [c] Referenced to TSP. [d] Previously assigned (ref 2). [e] $^3J_{C-P}$ = 5.83 Hz. [f] $^3J_{C-P}$ = 9.10 Hz.

(which will be shown to correspond to C25) exactly overlap. A cross peak between these two overlapping methyl group signals and a resonance at 2.65 ppm is tentatively assigned as the $C54H_3$/C18H cross peak. (Multiple bond ^1H–^{13}C connectivities between the C54 methyl protons and carbon C18 and between C18H and carbon C54 confirm this assignment, vide infra.) C18H has a cross peak with methyl protons C20 which show NOE connectivity to methyl protons C25. This methyl group has a cross peak with proton C3, which connects to $C35H_3$. Methyl protons C35 show NOE connectivity to methyl protons C36. A cross peak between $C36H_3$ and C8H would complete the ^1H connectivity around the corrin ring. Unfortunately, the high-field doublet component of C37H″ overlaps exactly with the resonance of methyl protons C36, and both C37H″ and $C36H_3$ are expected to have a cross peak with C8H. Although a cross peak between these signals is observed, the C37H″/C8H NOE should be much stronger than the $C36H_3$/C8H NOE, and the presence of the latter NOE cannot be determined unequivocally. Assignment of all other proton resonances follows from scalar connectivity (Figure 2 and supplementary figures) with the protons assigned above and from interpretation of the remaining NOE cross peaks. Any remaining doubts about the assignments obtained this way can, as will be shown later, be removed by detection of two- and three-bond proton–carbon connectivity. Furthermore, the results agree with previous partial assignments[2] of the ^1H spectrum of coenzyme B_{12} (Table II). All observed NOE connectivities are given in Table I.

Assignment of the ^{13}C NMR Spectrum

With the ^1H assignment complete, assignment of the ^{13}C spectrum can be obtained straightforwardly by using 2D ^1H–^{13}C shift correlation methods. The low solubility of coenzyme B_{12}, however, causes rather poor ^{13}C NMR sensitivity and makes the recording of a conventional one-bond 2D shift correlation spectrum time consuming, unless very large sample volumes are used. As we will demonstrate below, a convenient alternative approach is to use the large sensitivity enhancement that can be obtained by using the ^1H-detected heteronuclear multiple-quantum coherence (HMQC) for correlation of ^1H and ^{13}C chemical shifts.

^1H-Detected Heteronuclear Multiple-Quantum Coherence. Indirect detection of low-γ nuclei, by monitoring their effect on the more intense ^1H signals, can provide a large enhancement in sensitivity relative to direct detection methods. A number of experiments with different advantages and disadvantages have been proposed for this purpose.[9,11,13,14,33,34] We find the following sequence most convenient for practical use

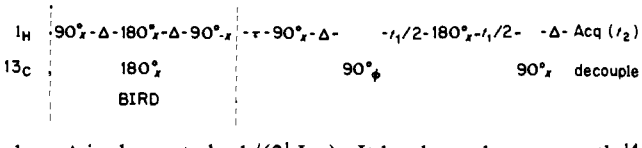

where Δ is chosen to be $1/(2^1J_{CH})$. It has been shown recently[14] that this scheme provides a very rapid and effective way for correlating ^1H and ^{13}C chemical shifts. The first part of the sequence, a BIRD pulse,[35,36] inverts all protons not coupled to ^{13}C and leaves protons coupled to ^{13}C unaffected. A time τ later, the actual HMQC experiment is started. The value for τ (in our case 300 ms) is adjusted to minimize signals from protons not coupled to ^{13}C,[14] facilitating the suppression of these unwanted signals and alleviating dynamic range problems. The phase, ϕ, is cycled x, y, $-x$, $-y$, while the receiver phase is +, +, −, −, in consecutive scans. The data acquired for odd- and even-numbered scans are stored in separate memory locations, and the data are processed in the standard fashion[29,30] to obtain phase-sensitive absorption mode spectra. In principle, the observed ^1H signals are modulated

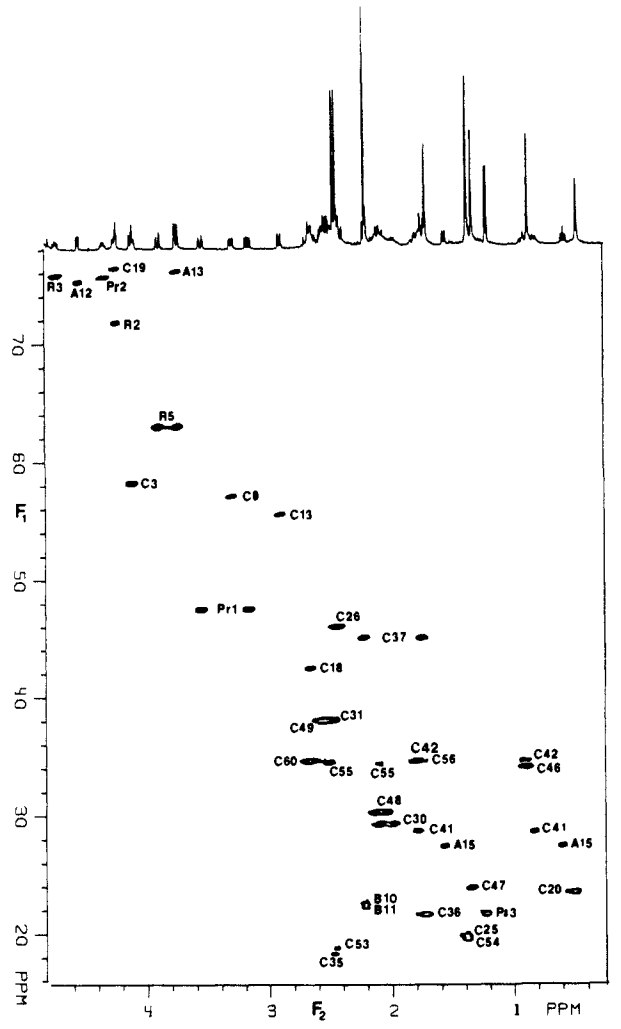

Figure 5. Part of the high-field absorption mode ^{1}H-detected ^{1}H–^{13}C shift correlation spectrum of coenzyme B_{12}. The F_2 coordinate of a resonance indicates the ^{1}H chemical shift, and the F_1 coordinate indicates the shift of the ^{13}C nucleus directly attached to this proton. The conventional 1D ^{1}H spectrum corresponding to the displayed region of the 2D spectrum is shown at the top of the figure. The total measuring time was 5 h. For further experimental details, see the Experimental Section. Direct connectivity between the protons and the carbons downfield from 80 ppm are shown in a supplementary figure.

not only in amplitude by the ^{13}C shifts, but also slowly in phase by the homonuclear scalar ^{1}H coupling. For acquisition times in the t_1 dimension that are much shorter than $1/J_{HH}$, the line shapes will not be affected seriously. We typically use 20–30-ms acquisition times in the t_1 dimension which normally provide more than adequate resolution in the ^{13}C dimension.

^{13}C decoupling during data acquisition is employed by using WALTZ-16 modulation.[37] For our probe, the highest safe ^{13}C decoupling power level (12 W) produces a 3.0-kHz rf field strength, sufficient to decouple an 8-kHz ^{13}C bandwidth (64 ppm on our 500-MHz spectrometer). To cover the entire ^{13}C spectral width two experiments were performed, one ranging from 15 to 85 ppm (Figure 5) and one ranging from 85 to 155 ppm (supplementary figure). From expanded displays of these spectra, the chemical shifts of all ^{13}C nuclei attached to protons (assigned earlier) can be measured directly. Resonance assignments obtained this way are tabulated in Table II. Due to the overlap in the ^{1}H spectrum, some of the ^{13}C resonances (e.g., B10 and B11 or C25 and C54) cannot be assigned unambiguously on the basis of the HMQC spectra alone. As will be shown later, correlation via multiple-bond J_{CH} coupling can be used to resolve these ambiguities.

Sensitivity of ^{1}H-Detected Heteronuclear Multiple-Quantum Coherence. There has been some confusion about the sensitivity enhancements that are obtainable by using ^{1}H-detected heteronuclear shift correlation. Here, we compare two heteronuclear shift correlation experiments: the conventional experiment with direct detection of the low-γ nucleus, and the analogous ^{1}H-detected HMQC scheme discussed above. Neglecting rf loss factors, the sensitivity of a nucleus is proportional to γ^3. The ratio of the magnetogyric constants of the proton (γ_H) and the low-γ nucleus (γ_L) is defined as ϵ ($\epsilon = \gamma_H/\gamma_L$). In the conventional 2D experiment ^{1}H spin polarization is transferred to the low-γ nucleus, enhancing the sensitivity by a factor of ϵ. This reduces the advantage of the ^{1}H-detected experiment to a factor of ϵ^2. A complication of the comparison of sensitivities of the two experiments is caused by the different decay constants of the signals acquired during data acquisition. For the ^{1}H-detected experiment, optimum sensitivity is often obtained by using a rather short data acquisition time in the t_2 dimension (about $1/2J_{HH}$) and strong digital filtering with a Gaussian function to avoid appearance of homonuclear J coupling, which would distribute the intensity of one proton over all homonuclear multiplet components. The effective data acquisition time is therefore only about 50 ms in the HMQC experiment. In the conventional experiment, the decay constant of the low-γ nucleus can be up to 10 times larger, intrinsically yielding a factor of $10^{1/2}$ in sensitivity enhancement for the conventional experiment. For larger molecules, however, transverse relaxation times of the low-γ nuclei are often rather short, and moreover, a long data acquisition time in the conventional experiment often requires unacceptably large data matrices. Therefore, in practice, different decay constants do not influence the sensitivity dramatically. For CH_2 and NH_2 groups, only one-half of the total proton magnetization is transferred to the low-γ nucleus in the conventional 2D experiment. For methyl groups, only one-third of the ^{1}H magnetization results in net ^{13}C magnetization. In contrast, the HMQC experiment utilizes the full proton magnetization of NH_2, CH_2, and CH_3 groups, providing extra enhancement factors of 2, 2, and 3, respectively. For direct detection of low-γ nuclei, large sample volumes can be used conveniently, yielding significant increases in sensitivity. For the ^{1}H-detected HMQC experiment, large sample volumes do not necessarily increase sensitivity because of the resulting severe dynamic range problems and practical problems of decoupling the low-γ nucleus. In conclusion, if sample quantities are the main factor limiting sensitivity, the HMQC experiment provides a gain of about 16 or 100 for ^{13}C or ^{15}N detection, respectively, relative to the conventional 2D experiment. An extra factor of 2 applies for NH_2 and CH_2 groups, and an extra factor of 3 applies for methyl groups.

^{1}H-Detected Multiple-Bond Heteronuclear Multiple-Quantum Coherence. The HMQC experiment described above does not provide assignment information for nonprotonated carbons. Also, for the case of exactly overlapping ^{1}H resonances, the HMQC experiment does not provide an unambiguous ^{13}C resonance assignment. Here we show how $^2J_{CH}$ and $^3J_{CH}$ couplings can be used to generate multiple-bond heteronuclear multiple-quantum coherence which then provides the equivalent of a heteronuclear shift correlation spectrum via long-range couplings.[15] This HMBC experiment can be considered a more sensitive alternative to the H,C-COLOC experiment.[38] The pulse sequence of the HMBC experiment is

$$^1\mathrm{H}\quad 90°_x\text{–}\Delta_1\text{–}\quad\text{–}\Delta_2\text{–}\quad\text{–}t_1/2\text{–}180°_x\text{–}t_1/2\text{–}\quad\text{–Acq.}(t_2,\psi)$$

$$^{13}\mathrm{C}\qquad\qquad 90°_{\pm x}\quad 90°_{\phi}\qquad\qquad\qquad 90°_x$$

The first $90°_{\pm x}$ pulse, applied at time Δ_1 ($=1/2^1J_{CH}$) after the first 90° proton pulse, serves to suppress one-bond correlations in the 2D spectrum.[39] This 90° ^{13}C pulse generates heteronuclear multiple-quantum coherence for protons directly attached to ^{13}C, which is removed from the spectrum by alternating the phase of the pulse along the $\pm x$ axis, without changing the phase of the receiver. The second 90_{ϕ} ^{13}C pulse, applied at time Δ_2 later, creates the multiple-bond, multiple-quantum coherence of interest. In principle, the optimum choice of Δ_2 is $1/2^nJ_{CH}$, where $^nJ_{CH}$ is the long-range coupling constant of interest. However, in practice, decay of the ^{1}H magnetization occurs due to transverse relaxation

and unresolved homonuclear couplings, and a somewhat shorter value for Δ_2 (50–80 ms) is found to be optimal. In contrast to the HMQC experiment discussed earlier, the dephasing due to homonuclear J coupling is generally quite large during this long delay period, which makes obtaining absorptive 2D spectra impossible. The use of purge pulses and z filters, as recently proposed by Frey et al.,[40] degrades the sensitivity unacceptably in this application and also makes the suppression of proton signals not coupled to ^{13}C more difficult. Therefore, the experiment is most easily executed by using artificial phase modulation,[41-43] by cycling the phases ϕ and ψ simultaneously along the x, y, $-x$, and $-y$ axes. The spectrum is then displayed in the absolute value mode.

At the beginning of the detection period, the magnetization originating from multiple-bond, multiple-quantum coherence is in antiphase. A sine bell or convolution difference filter in the t_2 dimension provides close to matched filtering, optimizing sensitivity. We use a relatively short data acquisition time in the t_1 dimension (20–40 ms) with little or no digital filtering. At least one "zero fill" in the t_1 dimension is used prior to Fourier transformation. The resulting truncation artifacts in the F_1 dimension do not constitute a problem at the low signal-to-noise levels typically encountered. Since the presence of a ^{13}C nucleus does not significantly affect the longitudinal relaxation rate of a proton two or more bonds removed, the repetition rate of the experiment is determined by the T_1 relaxation rate measured in a conventional experiment. We prefer to use a relatively short repetition rate, equal to about twice the T_1 of the methylene protons in the molecule. As for the HMQC experiment, methyl protons give signals of much higher intensity than other protons. In the large variety of compounds we have studied so far with the HMBC method, we always find connectivity to the carbon adjacent to the methyl group and all carbons that are three bonds removed from the methyl protons. Most difficult to observe are the long-range connectivities to protons that have a broad, poorly resolved multiplet structure, as often encountered for nonequivalent geminal protons that are also coupled to a number of other protons.

In an earlier communication,[15] we presented the multiple-bond correlation spectrum for the high-field proton and the high-field carbon resonances of coenzyme B_{12}. A similar spectrum, recorded under slightly different conditions, is shown in Figure 6. This spectrum shows the connectivity between the C54 methyl protons and C18. Connectivity between C18H and the C54 carbon is also observed, outside the spectral region displayed in Figure 6, removing the ambiguity in the NOE data mentioned earlier. Also visible in Figure 6 is the connectivity between C13H and C46, whereas no connectivity was observed between C13H and C47. This indicates that C13H has a larger coupling with C46 than with C47, in agreement with the cis configuration between C46 and C13H and the gauche configuration between C13H and C47.

^1H correlation with the downfield carbon signals (below 90 ppm) is shown in Figure 7. As mentioned above, the methyl resonances provide intense correlations via long-range couplings but also present the highest level of incompletely suppressed signal from protons not coupled to ^{13}C, resulting in severe ridges of t_1 noise. Plots with different contour levels are needed to display both the connectivity to methyl groups and connectivity to other protons that resonate in the same upfield region of the ^1H spectrum. Most nonprotonated carbons can be easily assigned from such a correlation spectrum. Consider, for example, the adenosyl ring. The relevant correlations are shown in Figure 7a. A8H and A11H show connectivity to the same carbon resonance at 151.8 ppm, which then must be A4. A8H also shows connectivity to a resonance at 121.8 ppm, which then must be A6. Assignment of the benzimidazole carbons follows in a similar fashion. Because R1H does not show connectivity to B8, distinction between the B8 and B9 carbon resonances is not immediately obvious. However, since two-bond J_{CH} couplings in aromatic systems are usually quite small,[44] whereas three-bond couplings are usually

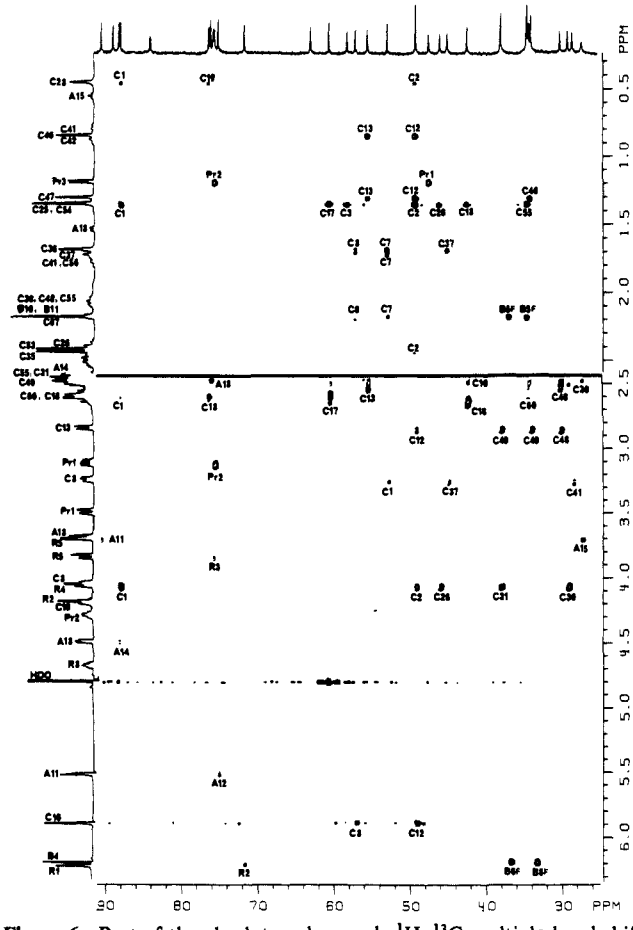

Figure 6. Part of the absolute value mode ^1H–^{13}C multiple bond shift correlation spectrum of coenzyme B_{12}. The 1D ^{13}C spectrum (obtained with a 50-mg sample on a 400-MHz spectrometer) and the 1D ^1H spectrum are shown along the top and left side of the spectrum, respectively. Correlation peaks are due to multiple bond connectivity between ^{13}C nuclei (labeled with the peak in the 2D spectrum) and protons (labeled in the 1D ^1H spectrum). For example, the three peaks near the top of the 2D spectrum indicate long-range coupling between methyl protons C20 and carbons C1, C19, and C2. The lowest contour level for the part of the spectrum below the drawn line in the spectrum is 3 times lower than for the region above the drawn line. Resonances folded in the ^{13}C dimension are labeled "F".

4–6 Hz, it is assumed that the connectivity between B7H and a carbon at 141.0 ppm stems from coupling to B9. Similar arguments are used for distinguishing carbons B5 and B6.

Connectivity around the corrin ring is also easily established from the HMBC spectra of Figures 6 and 7. Starting again at C10H, we find correlations with C9, C11, C8, and C12. Methyl protons C46 are coupled to C12 and to C13. C13H is coupled to C14. Methyl protons C53 are coupled to C14, C15, and C16. Methyl protons C54 are coupled to C16, C17, and C18. C18H is coupled to C19 and C1. Methyl protons C25 are coupled to C1, C2, and C3. C3H is coupled to C4, and methyl protons C35 are connected to C4, C5, and C6. Finally, methyl C36 completes the connectivity around the corrin ring by coupling to C6, C7, and C8. All multiple-bond ^1H–^{13}C connectivities observed in this study are given in Table I.

Assignment of the Carbonyl Resonances. Assignment of the carbonyl resonances was the most difficult part of the ^{13}C assignment because (a) only long-range connectivity information could be used and (b) the protons that have long-range couplings to the carbonyls are all in very crowded spectral regions. Nevertheless, as will be shown below, unequivocal assignments can be made. All but one of our carbonyl assignments confirm earlier assignments made on the basis of chemical evidence.[1]

In the 1D ^{13}C spectrum (not shown), the resonance at 178.7 ppm has an intensity corresponding to two carbons. In Figure 7b it is seen that protons $C35H_3$ and C3H are coupled to a

(43) Bax, A. *Two-Dimensional Nuclear Magnetic Resonance in Liquids*; Reidel: Boston, 1982; pp 59–61.
(44) Hansen, P. E. *Prog. NMR Spectrosc.* **1981**, *14*, 175.

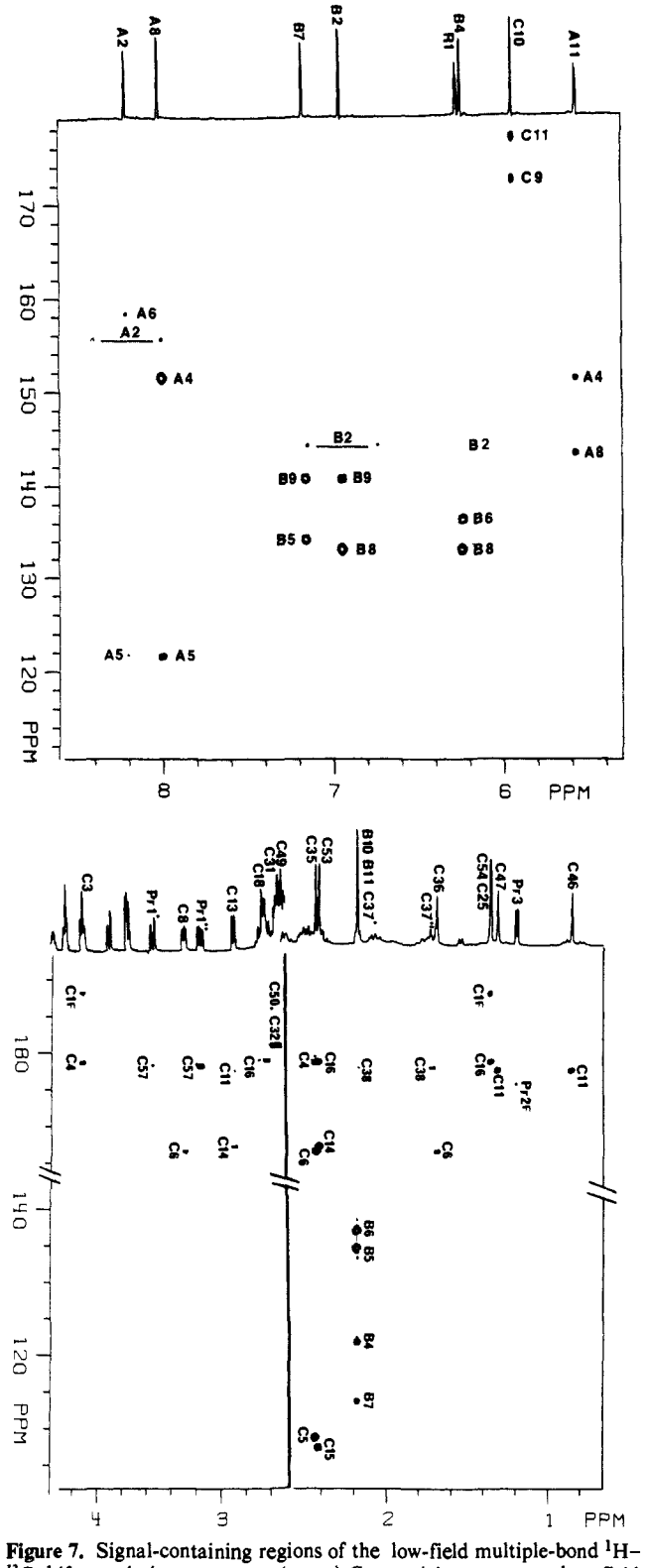

Figure 7. Signal-containing regions of the low-field multiple-bond ^1H–^{13}C shift correlation spectrum. (a, top) Connectivity to protons downfield from 5.4 ppm and (b, bottom) connectivity to protons upfield from 4.3 ppm. Signals above the drawn line in the 2D spectrum are displayed with a lowest contour level 4 times greater than for signals to the right of the drawn line. Incompletely suppressed correlations between protons and ^{13}C nuclei directly coupled to these protons are marked by horizontal bars.

resonance at 178.7 ppm, which then has to be C4. Methyl protons $C53H_3$ and $C54H_3$ are also coupled to a carbon at 178.7 ppm which then is assigned to C16. Similarly, C11 is identified by correlation with methyl protons $C46H_3$ and $C47H_3$. An expansion of the downfield ^{13}C region of Figure 7b, presented at lower contour levels, is shown in Figure 8. In this figure, protons $C60H_2$

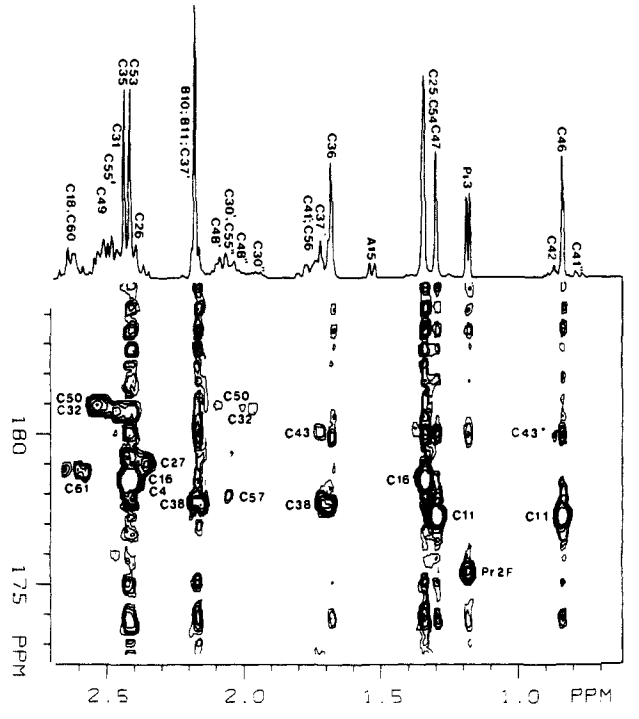

Figure 8. Expanded region of the spectrum of Figure 7b, displaying connectivity between protons and the carbonyl region of the ^{13}C spectrum. The lowest contour level is 5.5 times lower than that used in the right half of Figure 7b.

and C18H show connectivity to C61. Protons $C26H_2$ show connectivity to C27, and protons $C42H_2$ and C41H′ correlate with C43. C57 is identified via coupling with both R1 protons (Figure 7b) and also shows connectivity to C55H″. Proton C37H″ shows an intense correlation with a carbon at 177.9 ppm, which is then assigned to C38. The only unassigned carbon resonance, at 181.1 ppm, has an intensity corresponding to two carbons in the one-dimensional spectrum. Consequently, it must correspond to C32 and C50. The protons that are expected to show connectivity to these carbonyls ($C49H_2$, $C31H_2$, $C48H_2$, and $C30H_2$) also have nearly degenerate multiplets, but an intense correlation between the overlapping protons $C31H_2$ and $C49H_2$ and a carbon resonance at 181.1 ppm are observed in Figure 8. Moreover, three-bond connectivity is observed between this carbonyl resonance and protons C48 and C30. No other unidentified correlations remain, completing the ^{13}C spectral assignment. Assignments have been summarized in Table II.

Experimental Section

Coenzyme B_{12} (6.5 mg) (Sigma) was lyophilized once and dissolved in 0.35 mL of 99.96% D_2O (Merck) containing 10 mM phosphate buffer, p^{2}H 7.0. Experiments were performed by using a modified Nicolet NT-500 spectrometer, equipped with a Cryomagnet Systems[45] ^1H probe with a broad-band (^{15}N–^{31}P) decoupling coil for irradiation of ^{13}C. The temperature was 20 °C, and all experiments were carried out without sample spinning. All proton shifts are referenced to internal sodium 3-(trimethylsilyl)propionate (TSP). ^{13}C shifts are relative to external TSP in D_2O, as measured using a 50-mg sample in a 10-mm sample tube (2.5-mL sample volume) on a JEOL GX400 spectrometer (100.5-MHz ^{13}C frequency). For the ^1H-detected ^{13}C experiments, an approximate (±0.1 ppm) ^{13}C scale was obtained by multiplying the ^1H frequency that corresponds to 0 ppm by 0.251 449 54 (the $^{13}C/^1H$ frequency ratio in TSP).

^1H–^{31}P Spin–Echo Difference Spectroscopy. The spectrum of Figure 1 results from 128 scans, preceded by two dummy scans. A 75-ms delay between the 90° and 180° pulses and 3-Hz Gaussian line broadening were used. Four watts of ^{31}P decoupling power, corresponding to a 100-μs 90° pulse width, was used, and Waltz-16 ^{31}P decoupling[37] was employed during ^1H observation.

HOHAHA Spectroscopy. The spectrum of Figure 2 results from a 2 × 350 × 1024 data matrix size, with eight scans per t_1 value. The delay

(45) Cryomagnet Systems Inc., Indianapolis, IN 46203.

time between scans was 1.8 s, and the total measuring time was 1.5 h. An MLEV-17 mixing sequence of 52 ms preceded and followed by 2.5-ms trim pulses,[25] was used. Six watts of rf power provided a 35-μs 90° ^1H pulse width. Gaussian line broadening (6 and 9 Hz) was used in the t_2 and t_1 dimensions, respectively, to avoid truncation artifacts.

Spin-Locked NOE Spectroscopy. The spin-locked NOE spectrum resulted from a 2 × 350 × 1024 data matrix size, with 64 scans per t_1 value. The delay time between scans was 1.8 s, and the total measuring time was 12 h. The rf carrier was positioned at 5.2 ppm, and a 5-kHz rf field strength (50-μs 90° pulse width) was used. The mixing time (spin lock period) was 200 ms. For the spectra displayed in Figures 3 and 4, 12- and 10-Hz Gaussian line broadening was used in the t_1 and t_2 dimensions, respectively. The spectra were also inspected (data not shown) after processing with less severe line broadening to inspect overlapping cross peaks at higher resolution.

HMQC Spectroscopy. The one-bond ^1H–^{13}C shift correlation spectrum of Figure 5 resulted from a 2 × 300 × 1024 data matrix size, with 32 scans per t_1 value and a delay time between scans of 1 s, including the 300-ms τ period and a 100-ms acquisition period. The total measuring time was 5 h. Twelve watts of ^{13}C rf power was used to provide a 3.0-kHz ^{13}C rf field (84-μs 90° pulse width), sufficient to decouple an 8-kHz ^{13}C bandwidth (64 ppm). Two separate experiments, differing only in the ^{13}C rf carrier position, were carried out to cover the entire spectral range from 18 to 155 ppm. A 90_x–$180_{-x}270_x$ composite 180° pulse was used for the carbon pulse at the center of the BIRD pulse unit.

HMBC Spectroscopy. The multiple-bond ^1H–^{13}C shift correlation spectra resulted from 300 × 2048 data matrix sizes, with 128 scans (preceded by two dummy scans) per t_1 value and a delay time between scans of 1.5 s. Acquisition times were 24 and 220 ms in the t_1 and t_2 dimensions, respectively. The total measuring time was 16 h per spectrum. Fifteen watts of rf power was used to provide a 3.3-kHz ^{13}C rf field, and 70-μs ^{13}C pulse widths (corresponding to 82° rather than 90° flip angles) were used. Two separate experiments were carried out with the ^{13}C carrier positioned at 144 and 61 ppm, and the ^{13}C spectral width was 99.5 ppm in both experiments. Resonances outside the selected ^{13}C spectral window were also excited by the relatively short ^{13}C pulses and gave rise to weak resonances that were folded in the ^{13}C dimension. In both experiments Δ_1 and Δ_2 durations of 3.4 and 55 ms, respectively, were used. In the t_2 dimension, a sine bell filter and 4-Hz exponential line broadening were used prior to Fourier transformation. No digital filtering was used in the t_1 dimension.

Practical Suggestions

In this section we present some practical guidelines for using the newer types of 2D NMR techniques discussed in this paper. Of course, the ease of implementation of the various new techniques depends on the versatility of the particular spectrometer used. All experiments reported here were carried out on one of the earliest available Nicolet 500-MHz spectrometers, which required extensive hardware modification for implementation of the techniques discussed here. Some newer types of spectrometers may require little or no modification at all, however. We will mention the instrumental aspects that are critical for particular experiments and suggest simple procedures to check correct functioning of the pulse sequences.

HOHAHA Spectroscopy. To avoid probe damage, it is recommended that this experiment be executed with relatively low rf power. A 2F-Hz rf field strength should be sufficient to cover an F Hz spectral width, provided the carrier is positioned at the center of the spectrum. Attenuation of the high-power observe transmitter is not desirable since it may lead to attenuator damage or droop of pulse power during the relatively long mixing period. Correct functioning of the sequence is verified by first executing a simple spin lock experiment: $90_{\pm x}$–SL_y–Acq.(±), where SL_y is a regular spin lock, generated by defining a long pulse (50–200 ms) along the y axis. The phase of the observed spectrum should be independent of the length of the spin lock period (over the range of 5–300 ms). If the spin lock experiment does not function properly, this may be caused by an automatic rf shut-off device. The second step is to replace the SL_y spin lock by an MLEV-17 spin lock.[25] Again, the phase of the spectrum should be independent of the number of times that one cycles through the MLEV-17 sequence, and the decay of the signal should be as slow or slower than for the regular spin lock experiment. If the regular spin lock experiment functions properly but the MLEV-17 experiment does not, the problem may be inaccurate 90° phase shifts or unbalanced rf power for the various phases. We use a tuned class A Henry radio amplifier (maximum power 10 W) for providing the observe power. Tuned diodes (500-MHz) and a 500-MHz band-pass filter are used at the output of this amplifier, and an extra 76.76-MHz ^2H band-pass filter is used in the lock circuit to avoid perturbation of the lock by the ^1H irradiation.

Spin-Locked NOE Spectroscopy. As mentioned above, one first has to verify whether a regular spin lock experiment functions properly. The duration of the mixing time for molecules of interest, i.e., with $\omega_L\tau_c \approx 1$, is chosen between 100 and 300 ms. A 100-ms mixing time makes quantitation of the NOE effect easier, but a 300-ms mixing time usually will result in cross peaks closer to their maximum value and therefore provides close to optimum sensitivity for observing the presence of an NOE. As is the case for the regular NOESY experiment, the spin-locked NOE experiment should be used in the phase-sensitive mode, yielding absorptive spectra. Since some of the NOE peaks are quite small, care has to be taken that they are not swamped by base-line distortions of nearby intense resonances. We take the following precautions to avoid base-line problems. First, the time between the end of the spin lock period and the start of data acquisition is set to 20 μs. During the first half of this 20-μs period, the receiver electronics are gated off. Second, the audiofrequency filter bandwidth (3-dB attenuation) is set to about 1.4 times the spectral width. This causes the first couple of data points of the FID to be closer to their true value and therefore also minimizes base-line problems, at the expense of some extra noise near the edges of the spectrum. Incorrect functioning of the Fourier transform program[46] is also a cause of severe base-line distortion on most commercial spectrometers, but fortunately, this problem is not present in Nicolet software.

Resonances at opposite sides and equidistant from the carrier frequency will experience the same magnitude of the spin lock field. If these resonances correspond to scalar coupled protons, this will lead to a homonuclear Hartmann–Hahn effect during the spin lock period, which gives rise to artifacts in the 2D spectrum.[31] To minimize these effects, the carrier should be placed about 1 or 2 ppm downfield from the center of the spectrum and a relatively weak rf field employed.[31] For a spectral width of F Hz, a 1.5F-Hz rf field strength is sufficient.

HMQC Spectroscopy. The experiment is most easily implemented by first examining a ^{13}C-labeled compound. If ^{13}C decoupling during data acquisition affects the lock signal, this will give rise to poor cancellation of the protons attached to ^{12}C nuclei. We use two ^{13}C bandpass filters in series after the ^{13}C power amplifier and two ^2H band-pass filters in series between the probe and the ^2H preamplifier to remove this problem. In addition, an extra ^1H band-pass filter is used between the probe and the ^1H preamplifier. We find that a probe with a proton observe coil inside the low-γ irradiation coil gives results that are far better than those obtained by using a regular broad-band probe or a so-called "dual probe".

The dipolar coupling between a proton and a directly coupled ^{13}C nucleus is of about the same magnitude as the coupling between geminal methylene protons. Therefore, the protons of interest, attached to ^{13}C, relax efficiently, and a rather short delay time between scans can be used.

HMBC Spectroscopy. Since for ^{13}C the HMBC experiment is preferably executed without ^{13}C decoupling during data acquistion, the experiment may appear easier to implement. However the coupling constants used in the transfer process are very small (2–5 Hz), which makes effective conversion of ^1H magnetization into long-range heteronuclear multiple-quantum coherence and back into observable ^1H magnetization difficult. During the relatively long delays needed in this experiment, dephasing due to homonuclear ^1H coupling and decay due to transverse relaxation may also occur. Also, it is not possible to use a BIRD pulse for presaturation of the protons that are not coupled to ^{13}C as was done in the HMQC experiment. This makes suppression of protons not having a long-range coupling to ^{13}C difficult, and a very stable instrument is required to execute this

(46) Emonts, H. A. Thesis, Delft University of Technology, Holland, 1979.

experiment successfully. A relatively short delay (50 ms) between the 90° ^1H pulse and the first 90° ^{13}C pulse is close to optimum from a sensitivity point of view, but a longer delay (100 ms) makes the suppression of protons not coupled to ^{13}C easier. When working in D_2O solutions, we find accurate temperature control important for elimination of the unwanted ^1H signals. Because sample spinning modulates the quality factor (Q) of the receiver coil, better suppression of unwanted signals is usually obtained if the sample is not spun.

Discussion

Our study of coenzyme B_{12} illustrates the power of some of the newer types of 2D NMR techniques. Determination of long-range ^1H–^{13}C connectivity is crucial for providing complete proton and carbon assignments. This experiment provides information very similar to the 2D INADEQUATE experiment[47,48] but is several orders of magnitude more sensitive. In addition, this method allows the bridging of heteroatoms, not easily achieved with the INADEQUATE experiment. Assignment of the ^1H spectrum of coenzyme B_{12} was made using the new HOHAHA method in combination with the COSY and the spin-locked NOE experiments. However, some remaining ambiguities (for example, distinguishing between the C46 and C47 methyl protons) could only be resolved either by comparison of NOE data with the X-ray crystal structure or by using the long-range ^1H–^{13}C connectivity.

The results of previous studies led to correct but incomplete (about 50%) ^1H signal assignments. However, a relatively high number of incorrect ^{13}C signal assignments were made. It has been shown here, that unambiguous assignments of the ^{13}C spectrum can be made easily by correlation with the ^1H resonances. Use of the new techniques that use observation of the ^1H rather than the ^{13}C nucleus greatly enhances the sensitivity of ^1H–^{13}C shift correlation and makes it possible to use much smaller sample quantitites than hitherto possible.

Conformational changes in coenzyme B_{12} are universally recognized as being important in B_{12}-dependent enzymatic processes. The solution conformation of coenzyme B_{12} can be determined directly by interpretation of the 2D spin-locked NOE spectrum. A preliminary analysis shows no large conformational differences with the X-ray crystal structure, although some subtle changes can be observed. For other alkyl cobalamins we have found preliminary evidence for more dramatic structural changes. A discussion of these effects, together with a semiquantitative interpretation of the 2D NOE data, will be presented in a future paper.[49]

It has been demonstrated here that some of the newer types of 2D NMR techniques can be of crucial importance to make reliable spectral assignments. As will be demonstrated elsewhere, this new NMR approach provides a powerful new tool for structure elucidation of completely unknown compounds. Although most of the techniques discussed here may be somewhat more difficult than the now well-established COSY, NOESY, and heteronuclear shift correlation experiments, the new methods can provide information previously not available. We therefore expect that the approach outlined here will become widely used in the near future.

Acknowledgment. We thank Rolf Tschudin for continuous technical support, Dr. Laura Lerner for many useful comments during the preparation of the manuscript, and Dr. R. W. K. Lee (U.C.—Riverside) for helpful comments. L.G.M. thanks the NIH for financial support, Grant GM 29225. L.G.M. thanks the NIH for financial support, Grant GM 29225.

Registry No. Coenzyme B_{12}, 13870-90-1.

Supplementary Material Available: HOHAHA spectra showing the ^1H–^1H J-coupled networks, the COSY spectrum, and the downfield ^{13}C region of the ^1H–^{13}C HMQC spectrum (5 pages). Ordering information is given on any current masthead page.

(47) Bax, A.; Freeman, R.; Frenkiel, T. A. *J. Am. Chem. Soc.* **1981**, *103*, 2102.

(48) Bax, A.; Freeman, R.; Frenkiel, T. A.; Levitt, M. H. *J. Magn. Reson.* **1981**, *43*, 478.

(49) Summers, M. F.; Bax, A.; Marzilli, L. G., unpublished results.

First Observation of Electroluminescence at the p-Type Semiconductor/Electrolyte Interface Caused by Electron Injection: Energetics of Adsorbed Hydrogen at the p-GaAs Electrode

Kohei Uosaki* and Hideaki Kita

Contribution from the Department of Chemistry, Faculty of Science, Hokkaido University, Sapporo 060, Japan. *Received February 4, 1986*

Abstract: Electroluminescence (EL) due to a band-to-band transition was observed at the p-GaAs/1 M NaOH and p-GaAs/0.5 M H_2SO_4 interfaces just after the potential was pulsed from the strong negative bias to the potential near the flat band potential. The integrated EL intensity increased with the increase of the cathodic pulse width, i.e., the charge passed during the cathodic pulse, but became constant when the pulse width was longer than ca. 2 ms and the cathodic charge was larger than 350 $\mu C \cdot cm^{-2}$. These results and other evidence suggest that the EL of this system is caused by electron injection from the adsorbed hydrogen atom formed during the cathodic pulse as an intermediate of the hydrogen evolution reaction. The quenching of the EL and the increase of hydrogen evolution reaction rate in the dark by the surface treatment by Ru^{3+} mean that the energy level of adsorbed hydrogen at Ru^{3+} treated p-GaAs is below the conduction band edge at the surface.

The electroluminescence (EL) measurement is proved to be useful for the study of the electrochemical reaction mechanism at semiconductor electrodes,[1] particularly to probe the reaction intermediates[2] and the surface states of semiconductors.[3] EL

0002-7863/86/1508-4294$01.50/0 © 1986 American Chemical Society